

GT2003-38304

## THE TRANSITION MECHANISM OF HIGHLY-LOADED LP TURBINE BLADES

R. D. Stieger<sup>†</sup> and H.P. Hodson  
Whittle Laboratory  
Cambridge University Engineering Department  
Cambridge  
England

### ABSTRACT

A detailed experimental investigation was conducted into the interaction of a convected wake and a separation bubble on the rear suction surface of a highly loaded low-pressure (LP) turbine blade. Boundary layer measurements, made with 2D LDA, revealed a new transition mechanism resulting from this interaction. Prior to the arrival of the wake, the boundary layer profiles in the separation region are inflexional. The perturbation of the separated shear layer caused by the convecting wake causes an inviscid Kelvin-Helmholtz rollup of the shear layer. This results in the breakdown of the laminar shear layer and a rapid wake-induced transition in the separated shear layer.

### INTRODUCTION

Historically, turbomachinery blading has been designed using a combination of steady cascade measurements and steady computational tools. These design procedures lead to design rules that limited boundary layer deceleration to avoid laminar separation and the associated loss penalties. Schulte and Hodson [1] showed that the periodic passing of turbulent wakes affected the separation bubble on a modern LP turbine blade and reported a reduction in profile loss due to wake passing for some flow conditions. Schulte and Hodson [2] subsequently explained this by presenting hot film measurements showing that turbulent spots induced by the wake upstream of the separation point prevented the boundary layer from separating. The calmed regions that follow the turbulent spots were also shown to be responsible for suppressing separation due to their full velocity profiles.

Loss reductions are intimately linked to the relative portions of the blade surface covered by laminar, turbulent, calmed and separated flow. This is true for steady and unsteady flows. As the Reynolds number decreases, the steady flow losses rise due to the increased extent of separation. In the

wake passing case, the separation is periodically suppressed by the turbulent and calmed flow. The flows associated with the turbulent and calmed periods produce less entropy than the steady separation and this leads to a reduction of loss in the time-mean. The loss reduction is thus also dependant on the reduced frequency and it is fortuitous that the reduced frequency in LP turbines is typically in the correct range for loss reductions.

Armed with this improved understanding of unsteady transition, the traditional steady flow design rules that limited boundary layer diffusion were challenged. A new generation of blade profiles was designed based on the extensive experimental work of Curtis et al. [3] and Howell et al. [4]. These “high lift” LP turbine blade profiles were reported to reduce the number of blades in the LP turbine by 20% (Cobley et al., [5]) thus reducing the cost of ownership by simultaneously reducing weight and manufacturing costs without an efficiency penalty. The pitch to chord ratio and Zweifel lift coefficient of these blades are approximately unity. The advent of “Ultra High Lift” blades reported by Haselbach et al. [6] lead to a further reduction in the number of blades of 11%. However, such increases in blade loading were only possible when accompanied by the extensive experimental validation of Brunner et al. [7], Howell et al. [4] & [8].

Despite significant reductions in the number of blades, the fundamental transition mechanisms involved in reducing losses are not fully understood. Although the understanding of bypass transition has been greatly enhanced by the DNS calculations of Wu et al. [9] and the models of Johnson [10], the effects of separated boundary layers have not been adequately accounted for. The correlations of D’Ovidio et al. [11]-[12] have attempted to provide a workable solution but a lack of physical insight into the transition process resulting from the interaction

---

<sup>†</sup> Current address: Rolls-Royce plc, Derby, UK

of a convected wake and laminar separation remains a limiting factor.

In order to gain a better understanding of the wake boundary layer interaction a series of boundary layer traverses were performed using 2D LDA in a low speed bar passing cascade. The results, presented here provide new insight into the wake-induced transition mechanisms found on LP turbine blades with inflexional boundary layer profiles associated with separation bubbles. The boundary layer state is investigated at four representative phases during the wake passing cycle and this identifies the coherent structures in the boundary layer to be rollup vortices embedded in the boundary layer. These vortices are shown to originate from the breakdown of the separated shear layer that is triggered by the passing wake. Finally, the transition mechanism is described schematically and a new picture of wake-induced transition is presented.

### NOMENCLATURE

$C$	chord
$f_r$	reduced frequency $f_r = fC / U_b$
$H_{12}$	shape factor $H_{12} = \delta^* / \theta$
$P_{TKE}$	normalised production of TKE
$Re$	Reynolds number
$s$	surface distance
$s_0$	surface length
$s_b$	bar pitch
$s_c$	cascade pitch
$TKE$	normalised turbulent kinetic energy
$\overline{u'^2}, \overline{v'^2}$	normalised velocity variance components
$\overline{u'v'}$	normalised Reynolds stress
$U_b$	bar speed
$U_{98}$	normalised boundary layer edge velocity
$U, V$	normalised velocity components
$V_{x1}$	axial inlet velocity
$V_{2is}$	isentropic exit velocity
$x, y$	normalised linear dimensions
$\delta^*$	displacement thickness
$\delta_{TKE}$	TKE thickness
$\phi$	flow coefficient $\phi = V_{x1} / U_b$
$\theta$	momentum thickness
$\Omega$	normalised vorticity

### EXPERIMENTAL DETAILS

The measurements reported in this paper were performed on bar passing cascade facility at the Whittle laboratory of Cambridge University. The bar passing cascade, shown in Figure 1, simulates the unsteady wake passing environment of a turbomachine by traversing bars across the inlet flow. No attempt is made to simulate the unsteady potential field of adjacent blade rows. The bars are held between two nylon belts that run on two sets pulleys. The pulley system is driven through a belt drive by a DC motor. The configuration of the bar passing cascade required that the top and bottom walls of

the cascade be slotted to permit the passage of wake generator bars. These slots provide two additional passages to the flow and may result in a non-uniform inlet static pressure. In order to maintain inlet periodicity, an additional dummy passage was created on the suction side of the cascade. The throat of this dummy passage was then adjusted so that the periodicity of inlet static pressure was within 2.5% of the inlet dynamic head.

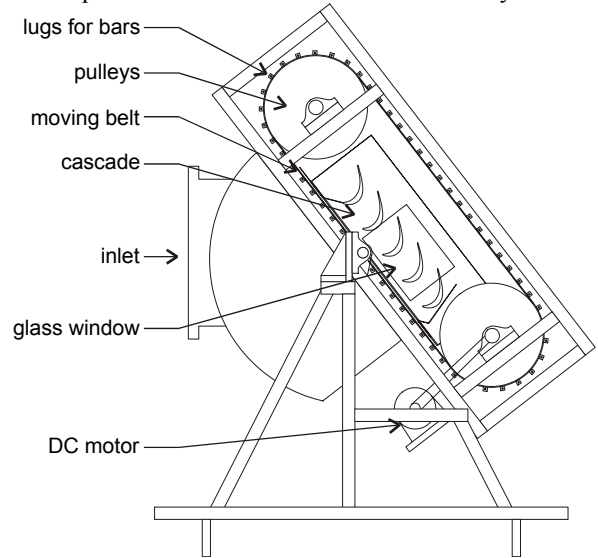


**Figure 1: Bar passing cascade with T106 profile.**

Details of the 5-blade cascade of the T106 profile are presented in Table 1. Under steady inflow, this profile has a separation bubble over the rear of the suction surface. This is evident in the measured isentropic surface velocity distribution shown in Figure 2.

Chord	[mm]	198
Blade stagger	[°]	59.3
Cascade Pitch	[mm]	158
Span	[mm]	375
Inlet flow angle	[°]	37.7
Design exit flow angle	[°]	63.2
Bar diameter	[mm]	2.05
Axial distance: bars to LE	[mm]	70
Flow Coefficient ( $\phi$ )		0.83

**Table 1: T106 bar passing cascade details.**

The unsteady wake-passing flow conditions were chosen to match those of a repeating stage of the T106 profile. The Reynolds number based on chord and time mean isentropic exit velocity of 12.6m/s was  $Re = 1.6 \times 10^5$ . The flow coefficient was  $\phi = 0.83$ . The bar pitch matched the cascade pitch so that  $s_b / s_c = 1$  ( $f_r = 0.68$ ). The bar diameter of 2.05mm was chosen to match the loss of a representative turbine blade and the axial gap is representative of that found in LP turbines. The inlet flow angle was set to the design value of  $\alpha_1 = 37.7^\circ$ .

The unsteady flow field was measured using a commercial 2D LDA system. LDA was selected due to the absence of probe interference and directional ambiguity associated with more traditional thermal anemometry. Light was supplied by a

5W Argon-Ion laser. The transmitting optics consisted of a Dantec FibreFlow unit incorporating a colour separator and Bragg cell. A 2D probe was used with a 1.95 beam expander and a lens of 500mm focal length. The optical configuration resulted in a measuring volume of  $0.077 \times 0.076 \times 1.0116$ mm for the 514.5nm beam and  $0.073 \times 0.072 \times 0.963$ mm for the 488nm beam. A backward scatter configuration was used and the receiving optics included a Dantec 55X35 colour separator and two Dantec 9057X0081 photo-multiplier tubes. Dantec BSA signal processors were used to process the photo-multiplier outputs.

Seeding of the flow was by means of smoke generated by a Dantec SPT smoke generator using Shell Ondina oil. The smoke was injected into the constant area section of the wind tunnel through the trailing edge of a streamlined injector tube. The point of injection was approximately 3m upstream of the test section and upstream of the honeycomb, contraction and final screens of the wind tunnel. The effect of the injector on the flow was thus immaterial. Phase Doppler anemometry measurements showed the characteristic size of the smoke particles used to be  $1.5 \mu\text{m}$ . At each traverse point a maximum of  $1 \times 10^5$  samples were collected in up to 60 seconds. This corresponded to a maximum of approximately 2500 wake passing cycles. Validated data rates typically varied from 1.5 to 5kHz. Two component measurements were made with both processors acting as coincidence masters. Final coincidence filtering was performed by software to reject any samples not detected by both photo-multipliers within a  $5 \mu\text{s}$  window corresponding to twice the sample record length.

Ensemble averaging of the LDA data was performed relative to a once per bar passing trigger. The wake passing period was divided into 128 time bins. Each coincident measurement was then assigned to a time bin according to its time relative to the trigger signal. The statistics of each time bin were then calculated with a residence time weighting to remove velocity bias as suggested by George [14].

A series of boundary layer traverses were performed on the suction surface of the central blade of the T106 LP turbine cascade. Each traverse was performed perpendicular to the local blade surface. The blade was painted matt black to minimise reflections from the intersecting laser beams except for a strip at midspan, which was left unpainted to avoid contamination of the static pressure tappings. For this reason the traverses were performed at 45% of the cascade span. Positioning of the measuring volume in the stream-wise direction was performed manually. The location of the surface was then found by traversing the LDA probe towards the blade surface in steps of 0.05mm while monitoring the photo-multiplier outputs. A peak in the photo-multiplier output indicates maximum light reflection, which occurs when the measuring volume intersects the wall. The wall was located with both the flow and rotating bars switched on. The first traverse point was 0.1mm from the blade surface and the first 16 points were exponentially distributed within the boundary layer. The final 4 of the 20 traverse points were evenly spaced

from the boundary layer edge to a point 16mm from the blade surface. 25 measurement locations were used in the streamwise direction. These were selected based on previous measurements.

## RESULTS

The isentropic surface velocity distribution derived from static pressure measurements on the cascade under wake passing conditions is also shown in Figure 2. It is apparent that in the time mean the wake passing suppresses the suction surface separation bubble. It is an unavoidable consequence of the experimental facility that the wake passing conditions introduce a small amount of incidence on the cascade as shown by the small differences between the steady and unsteady pressure distributions over the front of the blade. This incidence is small and has no significant impact on the blade surface boundary layers downstream of peak suction.

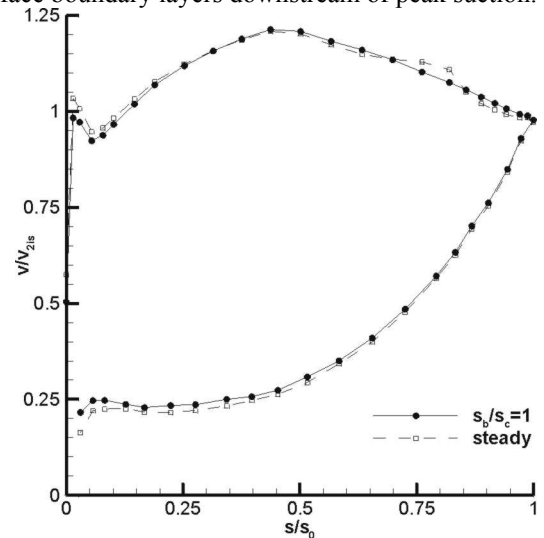


Figure 2: Isentropic surface velocity distribution measured on the T106 LP turbine cascade.

## A SPACE-TIME VIEW OF THE MEASURED BOUNDARY LAYER

The 2D LDA boundary layer data are presented as S-T diagrams in Figure 3 to Figure 5. To aid visualisation of the periodic unsteady process the data is copied onto three wake passing periods. The streamwise locations of the traverses are indicated by dots across the top of each of these figures.

### Boundary Layer Edge Velocity

The boundary layer edge is defined as the wall normal distance where the velocity is 98% of the maximum velocity measured in the local ensemble-average profile. The velocity at this point is taken as the boundary layer edge velocity. Measurements of the boundary layer edge velocity are non-dimensionalised by the isentropic exit velocity and plotted as an S-T diagram in Figure 3. Three trajectory lines denoted *A*, *B* and *E*, are drawn at the time average boundary layer edge velocity. Line *A* marks the peak velocity that results from

kinematics of the approaching wake (see Meyer [15] & Hodson [16]) and line *E* marks the minimum velocity, which occurs after the negative jet of the wake has passed. Line *B* is placed half way between lines *A* and *E* and is the approximate path of the centre of the wake.

Two further lines, labelled *C* and *D*, are drawn to mark two distinct structures originating along the wake centre at  $s/s_0 \approx 0.70$  and  $s/s_0 \approx 0.77$ . These perturbations to the boundary layer edge velocity have not previously been observed. They are attributed to the rollup vortices that form due to the interaction of the wake and separated shear layer. Further evidence of this will be presented later. These structures can be seen to follow trajectories slower than the local freestream, indeed, lines *C* and *D* are drawn with a trajectory of half the freestream velocity.

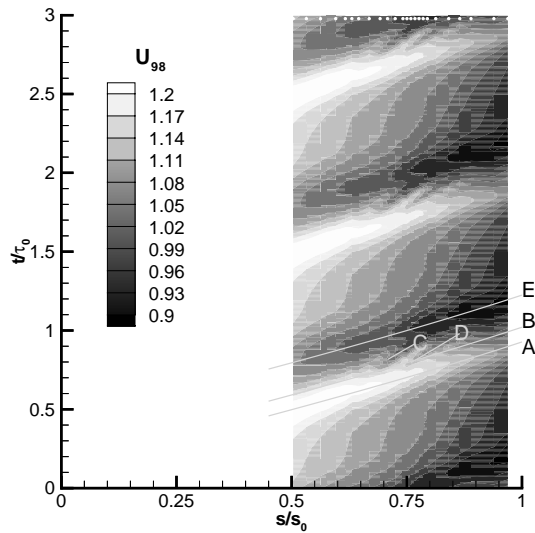


**Figure 3: Space-Time diagram of boundary layer edge velocity non-dimensionalised by  $V_{2is}$ .**

### Boundary Layer Shape Factor

The integral parameters were calculated from the measured ensemble average velocity profiles and the shape factor was calculated from these. An S-T diagram of the shape factor,  $H_{12}$ , is shown in Figure 4 with the trajectory lines and labels copied from Figure 3.

The wake path lies between lines *A* and *E*. Along line *A*, the outer part of the boundary layer is accelerated by the approaching wake. The increased velocity is not transmitted through the boundary layer instantaneously due to viscous effects. As a result the outer portion of the boundary layer accelerates more than the inner portion and the levels of  $H_{12}$  are increased between lines *A* and *B* downstream of  $s/s_0 = 0.60$ .

Along line *B*, the separating flow indicated by high  $H_{12}$  breaks down into wedge shaped regions originating at  $s/s_0 \approx 0.70$  and at  $s/s_0 \approx 0.77$ . These structures, which follow trajectory lies

*C* and *D*, were observed in Figure 3, and are sites of rapid break down of the high  $H_{12}$  flow to a turbulent boundary layer.

After the wake centre has passed over the region of high  $H_{12}$ , a more typical wake-induced transition occurs at  $s/s_0 = 0.75$  along trajectory *E*. This process, which lags behind the wake passing, may be a result of wake turbulence diffusing into the boundary layer and causing bypass transition. A characteristic wedge of turbulent boundary layer follows the wake-induced transition. The trailing edge of the wake induced turbulent strip is bound by line *F*, which is drawn at  $0.5U$ . The structures traced by trajectories *C* and *D* merge with the turbulent strip.

Line *G* is drawn with a trajectory of  $0.3U$ . This marks the approximate trailing edge of the calmed region, which is characterised by slowly increasing levels of  $H_{12}$  as the turbulent boundary layer relaxes back to the inflexional profiles of the separating boundary layer under a strong adverse pressure gradient. The calmed region controls the rear of the high  $H_{12}$  region.

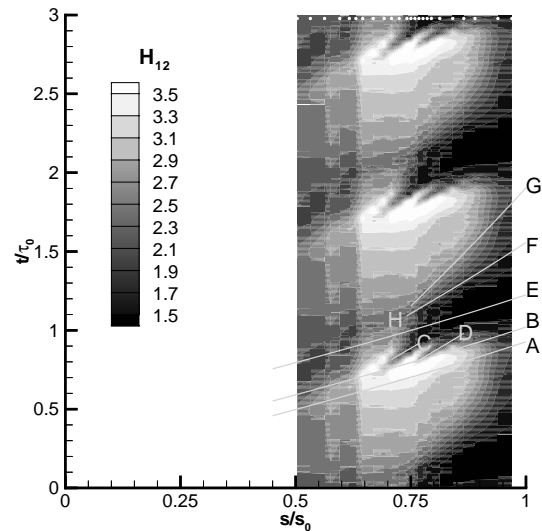


**Figure 4: Space-Time diagram of measured  $H_{12}$ .**

### TKE thickness

Due to practical constraints, the boundary layer state on turbomachinery blading is often inferred from measurements made with hot-film anemometers. The measurements are qualitative, however, as it is not the quasi-shear stress, but rather the random unsteadiness (ensemble average RMS), which is most useful in indicating the boundary layer state. D'Ovidio et al. [11]-[12] sought to recover the familiarity of using RMS as an indicator of boundary layer state while using all the data from hot wire boundary layer traverses. They adopted the Blackwelder parameter, which is an integral of the RMS fluctuations through the boundary layer non-dimensionalised by the boundary layer edge velocity. A similar approach is adopted for the current measurements. The

parameter  $\delta_{TKE}$  is defined as the integral of TKE through the boundary layer according to

$$\delta_{TKE} = \frac{1}{U_{98}} \int_{y=0}^{\delta_{98}} \frac{1}{2} (\overline{u'^2} + \overline{v'^2}) dy \quad (1)$$

An S-T diagram of  $\delta_{TKE}$  is shown in Figure 5 with the trajectory lines and labels from Figure 4 repeated. Upstream of  $s/s_0=0.70$ ,  $\delta_{TKE}$  is low throughout the wake passing cycle. This indicates that the boundary layer in this region is laminar throughout the wake passing cycle and is not significantly affected by the passing wakes. Downstream of this, the wake-induced path is characterised by very high levels of  $\delta_{TKE}$ , which originate along trajectory line *B*. The onset does not lag behind the wake and corresponds to the region where the structures *C* and *D* were observed in Figure 3 and Figure 4.

A second strip of elevated  $\delta_{TKE}$  is seen to originate at label *H*. This strip lags behind the passing of the wake and is a result of a wake-induced bypass transition that occurs once the wake turbulence has diffused into the boundary layer. As in Figure 4, the turbulent wedge may be identified by high levels of  $\delta_{TKE}$  between lines *E* and *F*, while the calmed region between lines *F* and *G* is characterised by low levels of  $\delta_{TKE}$  that extend to the trailing edge.

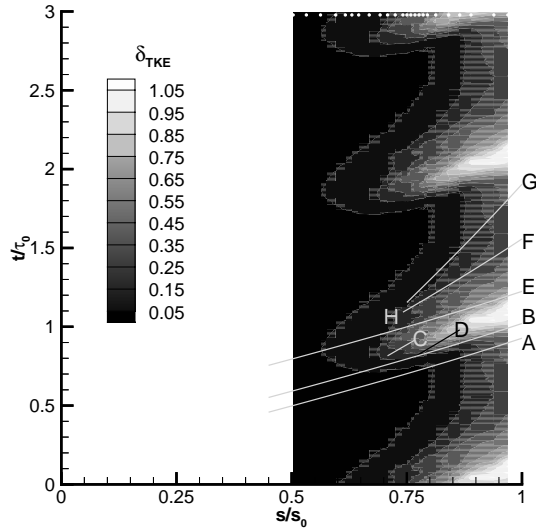


**Figure 5: Space-Time diagram of measured boundary layer TKE thickness.**

At the traverse location closest to the trailing edge, four distinct levels of  $\delta_{TKE}$  are distinguishable. The highest levels occur between lines *B* and *E* and originate from the interaction of the wake and the inflexional profiles of the separating boundary layer. The next highest region of  $\delta_{TKE}$  occurs between lines *E* and *F* and results from the turbulent strip formed by the wake induced bypass transition. The lowest region of  $\delta_{TKE}$  occurs between lines *F* and *G*. This region corresponds to the calmed region and shows that the calmed region persists to the

trailing edge. Finally between *G* and *A* of the following cycle the level of  $\delta_{TKE}$  is again elevated due to the natural transition that occurs once the influence of the calmed region has passed. It is worthy of note that the peak levels of  $\delta_{TKE}$  arise in the region of the interaction of the wake and separating boundary layer.

## UNSTEADY BOUNDARY LAYER DEVELOPMENT

Further details of the 2D LDA boundary layer traverses are presented in Figure 6 to Figure 9 as a series of snapshots of the boundary layer at illustrative phases through the wake passing cycle. At each of these phases, velocity vectors, perturbation velocity vectors and contour plots of vorticity describe the ensemble-averaged flow field. The perturbation velocity is the difference between the ensemble averaged and time averaged velocity fields and the vorticity is calculated with velocities normalised by  $V_{2is}$  and lengths normalised by *C* according to

$$\Omega = \partial V / \partial x - \partial U / \partial y \quad (2)$$

The *x* co-ordinate is in the axial direction and positive downstream.

The turbulent kinetic energy (TKE) is calculated from the measured velocity variance components normalised by  $V_{2is}^2$

$$TKE = \frac{1}{2} (\overline{u'^2} + \overline{v'^2}) \quad (3)$$

and is presented as contour plots. The production of TKE ( $P_{TKE}$ ) is calculated from the normalised mean velocity gradients and the normalised measured Reynolds stresses

$$P_{TKE} = -\overline{u'^2} \frac{\partial U}{\partial x} - \overline{v'^2} \frac{\partial V}{\partial y} - \overline{u'v'} \left( \frac{\partial U}{\partial y} + \frac{\partial V}{\partial x} \right) \quad (4)$$

## Boundary layer state before the interaction of the wake and inflexional profiles

Figure 6 shows the boundary layer prior to the interaction of the wake and separation bubble. The position of the centreline of the wake (trajectory line *B* in the S-T diagrams) is marked by a dot and is evident from the perturbation velocity vectors of Figure 6 (b), which shows the wake as a jet impinging on the blade surface and splitting into two streams along the blade surface. At this phase, the wake is upstream of the steady separation point, which is labelled *I*. Upstream of the separation point, the boundary layer is laminar and attached as seen by the profiles of the mean velocity vectors in Figure 6(a). The highest levels of vorticity are found on the wall and the levels of TKE and  $P_{TKE}$  are low. Downstream of *I* the boundary layer profiles become inflexional and the peak levels of vorticity are detached from the wall. A separated shear layer extends from *I* to 2. In the ensemble mean, this shear layer is not perturbed. This is confirmed by the smooth distribution of vorticity and the absence of wall normal components of the perturbation velocity vectors in this region. The separated shear layer reattaches downstream of 2. In this region, the velocity profiles become fuller and the levels of vorticity in the outer boundary layer reduce. Increased levels of TKE are also observed downstream of 2.

### Interaction of wake with separated shear layer

The interaction of the wake and inflexional profiles of the separated shear layer is shown in Figure 7. The wake is now located over the separated region with its centre marked by a dot. The perturbation velocity vectors of Figure 7(b) show that the wake passing over the separated shear layer has induced significant wall-normal velocity components.

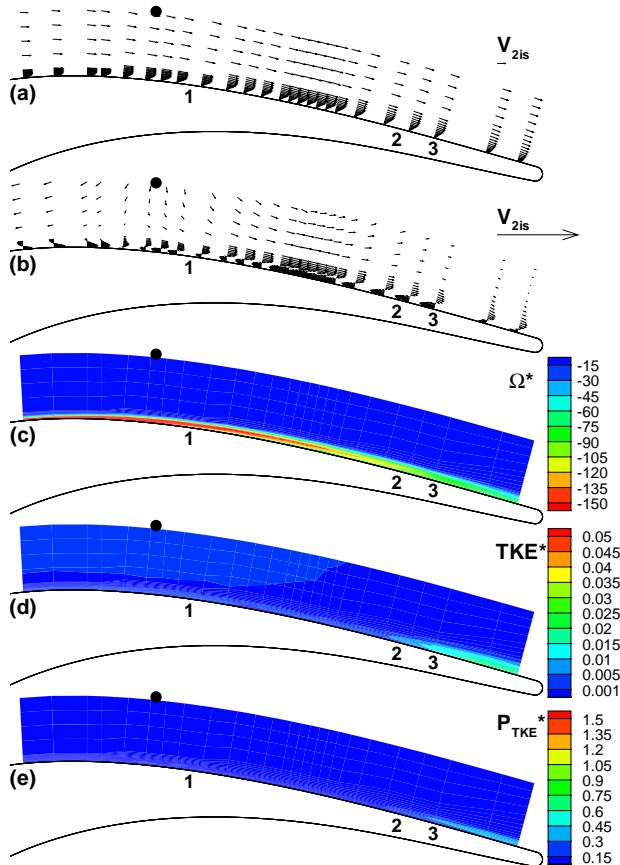


**Figure 6: Boundary layer structure prior to the wake arrival. Vector plots of (a) ensemble average velocity and (b) perturbation velocity. Contour plots of non-dimensional (c) vorticity, (d) turbulent kinetic energy and (e) production of TKE.  $Re=1.6 \times 10^5$ ,  $s_b/s_c=1$ .**

Between 4 and 6 the velocity profiles alternate between being inflexional and very full. This rapid change with distance along the blade surface is attributed to the rollup of the separated shear layer, which is induced by the wake. The profiles are thus the superposition of a vortex on the boundary layer profile. Indeed, rollup vortices may be identified at 4 and 5 both in the perturbation velocity vectors of Figure 7(b) and as localised regions of high vorticity embedded within the boundary layer in Figure 7(c).

The boundary layer edge can be inferred from the edge of the elevated vorticity region and the rollup vortices can be seen to thicken the boundary layer locally. The perturbation velocity vectors of Figure 7(b) show significant wall normal velocities associated with the rollup vortices. The rollup vortex with its

centre at 5 may be identified in the perturbation velocity vectors. It is clear that the rollup vortex at 5 induces large local flow curvature. Indeed, the unsteady surface pressure measurements of Stieger et al. [17] indicate that there is a strong local pressure field associated with the streamline curvature of roll-up vortices embedded in the boundary layer.

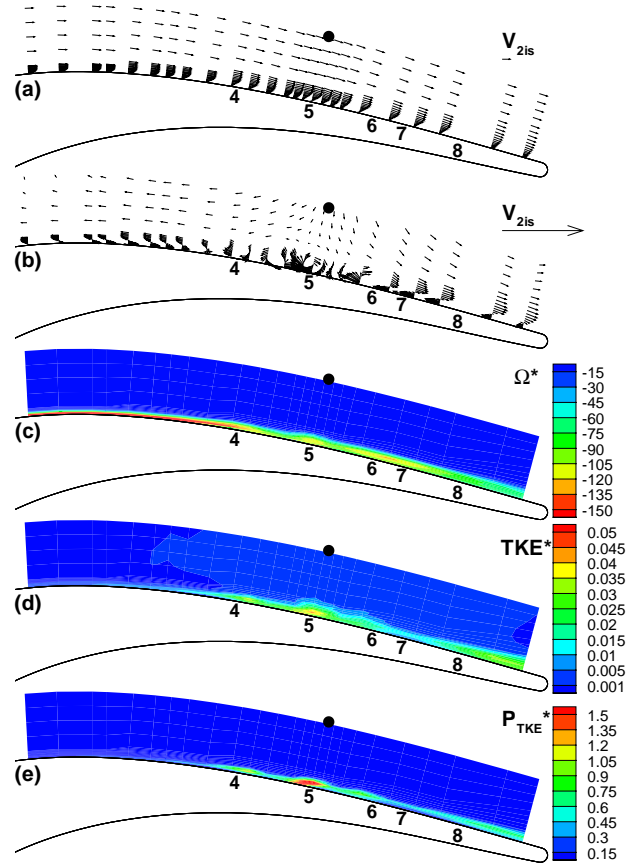


**Figure 7: Boundary layer structure during the interaction of wake and separated shear layer.  $Re=1.6 \times 10^5$ ,  $s_b/s_c=1$ .**

Downstream of the wake, between 6 and 8, the velocity profiles are inflexional and the vorticity contours again show a peak detached from the wall. This region has not yet been affected by the wake passing and there are no wall normal velocity components in the perturbation velocity vectors. The transition and reattachment of the inflexional profiles downstream of 8 occurs as for the previous phase shown in Figure 6.

Figure 7(d) shows contours of TKE. The elevated turbulence associated with the wake can be seen to extend from 4 to the trailing edge and the boundary layer TKE is elevated throughout this region. Regions of high TKE are distinguishable at labels 4 and 5. The highest levels of TKE are located at 5, which is the newly formed rollup vortex. The reduced levels of TKE at 7 correspond to the undisturbed inflexional profiles downstream of the wake. Downstream of

this, the elevated TKE is a result of the natural transition of the inflexional profiles.

The production of TKE, presented in Figure 7(e), follows the distribution of TKE with elevated production at the centre of the vortex. The peak levels of production are located at the centre of the vortex at 5. The natural transition downstream of 8 is also associated with elevated levels of TKE production

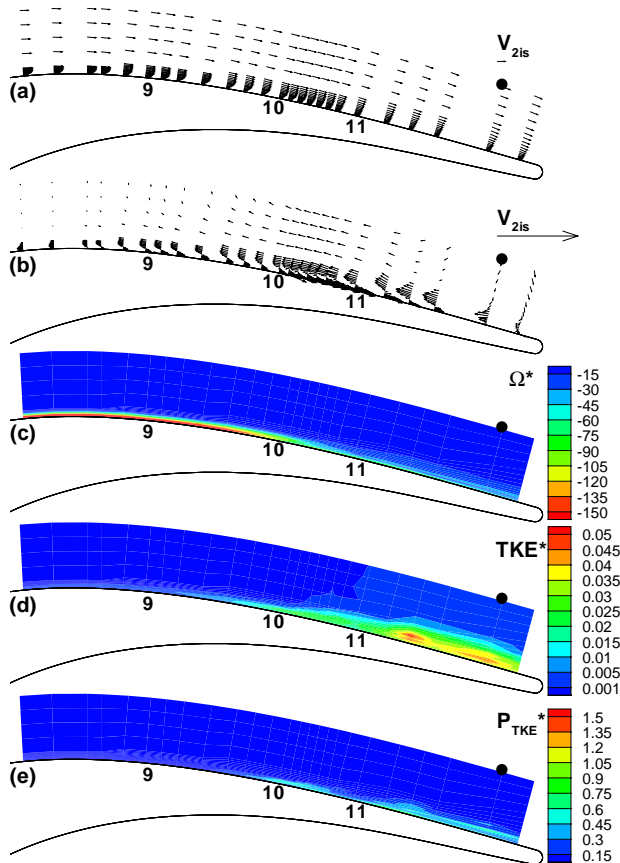


**Figure 8: Boundary layer structure through the wake induced turbulent strip.  $Re=1.6 \times 10^5$ ,  $s_b/s_c=1$ .**

### Boundary layer after wake interaction

Figure 8 shows the boundary layer state with the wake downstream of the separation region as indicated by the dot. Upstream of 9 the boundary layer profiles are laminar. Between 9 and 10 the boundary layer profiles have the shape of attached laminar profiles but the levels of TKE in this region are elevated as shown in Figure 8(d). This suggests that the profiles in this region are transitional.

Downstream of 10 the velocity profiles have a turbulent shape. However, the levels of TKE downstream of 11 are far higher than between 10 and 11. This is attributed to the breakdown of the rollup vortices. An isolated region of elevated TKE can be identified in Figure 8(d) at 11. Although not evident in the vorticity contours due to the coarse spacing of the traverses in this region, this is attributed to a rollup vortex and is accompanied by elevated TKE production. The

levels of production measured at the vortex centre are lower than those of Figure 7. The vortex is now further from the wall and so the boundary layer velocity gradients are smaller and this reduces the production of TKE at the vortex centre. The reduced streamwise resolution of the measurements downstream of 11 causes streaks in the contours and this prevents the identification of rollup vortices downstream of this location.

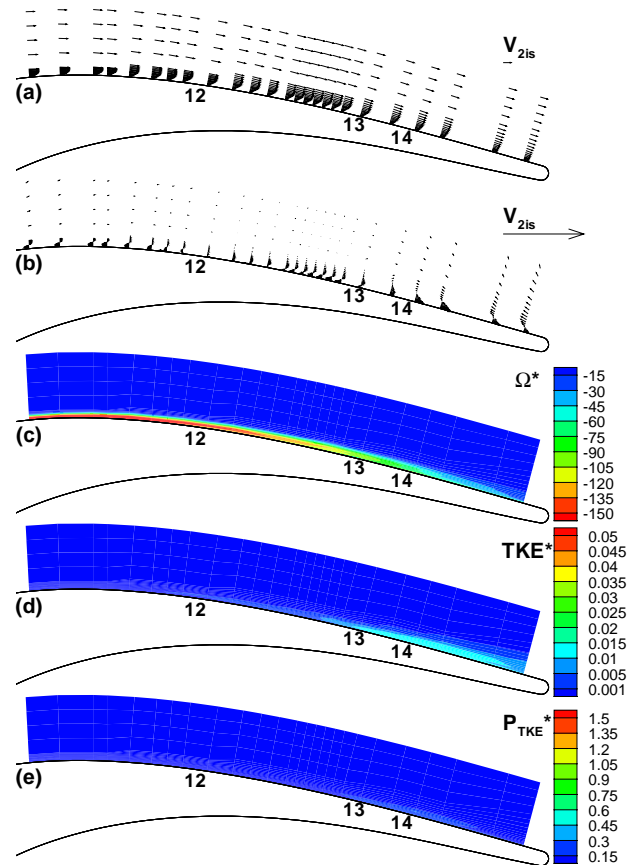


**Figure 9: Boundary layer structure in the calmed region.  $Re=1.6 \times 10^5$ ,  $s_b/s_c=1$ .**

The boundary layer between 10 and 11 is due to the wake-induced bypass transition and is characterised by elevated TKE together with elevated production and dissipation. The production in this region is of similar magnitude to that of the vortex centred at 11, however, the extent is smaller.

### Calmed boundary layer

After the passage of the wake, the boundary layer starts to relax back to its pre-transitional state. The phase shown in Figure 9 is representative of this process.

Upstream of 12 the boundary layer is laminar and attached with low levels of TKE. Between 12 and 13, the boundary layer is laminar and in the upstream part of this region, the profiles are becoming inflexional. This is emphasised by the vorticity peak moving away from the wall. Over the rear portion of the region between 12 and 13 the boundary layer

profiles are fuller and more like the calmed profiles that are observed between 13 and 14. The profiles between 12 and 13 describe the process whereby the calmed profiles become inflexional and begin to separate under the strong adverse pressure gradient.

The TKE is shown in Figure 9(d). The levels of TKE are observed to be low. The elevated region between 13 and 14 is due to the decaying boundary layer turbulence in the calmed region, while downstream of 14 the turbulence is due to the turbulent boundary layer.

The production of TKE is presented in Figure 9(e) and the levels are very low throughout the measurement domain with only a small region of low magnitude production at 14. These low levels of TKE production point to the loss reducing mechanism associated with the calmed region.

### MECHANISM OF WAKE-INDUCED TRANSITION

Based on the observed interaction of a convected wake and the separated shear layer of the re-establishing separation bubble on the T106 LP turbine cascade, it is possible to describe the mechanism whereby boundary layer transition occurs on highly loaded LP turbine blades with laminar separation.

The process is illustrated schematically in Figure 10. Schematic velocity profiles are shown at selected locations through the separation bubble and the dotted line indicates the separated shear layer. The wake is represented by a jet (negative jet) pointed towards the blade surface.

Figure 10(a) depicts the flow prior to the interaction of the wake and separated shear layer. The negative jet impinging on the blade splits into two streams, one pointed downstream which has the effect of accelerating the flow downstream of the approaching wake and one pointing upstream which retards the flow after the wake has passed. As the wake approaches the separation, the outer region of the boundary layer is accelerated. The inner region of the boundary layer responds more slowly than the freestream due to the fluid viscosity and as a result, the shear of the separation is intensified by the approaching wake.

As the wake convects over the separation, the wall normal component of the negative jet deforms the shear layer as shown in Figure 10(b). The separated shear layer is naturally unstable and the perturbation of the wake triggers an inviscid Kelvin-Helmholtz rollup as shown in Figure 10(c). The resulting rollup vortex convects at half the freestream velocity and so the wake, which convects with the freestream, moves ahead of the rollup and perturbs the separated shear layer further downstream. This results in the formation of further rollup vortices as shown in Figure 10(d). The vortices formed by the inviscid rollup of the shear layer rapidly breakdown to turbulence thereby causing boundary layer transition. After the passing of the rollup vortices and the turbulent boundary layer, a calmed region is formed and once the influence of the calming has subsided the boundary layer begins to separate once again. This is shown in Figure 10(e)

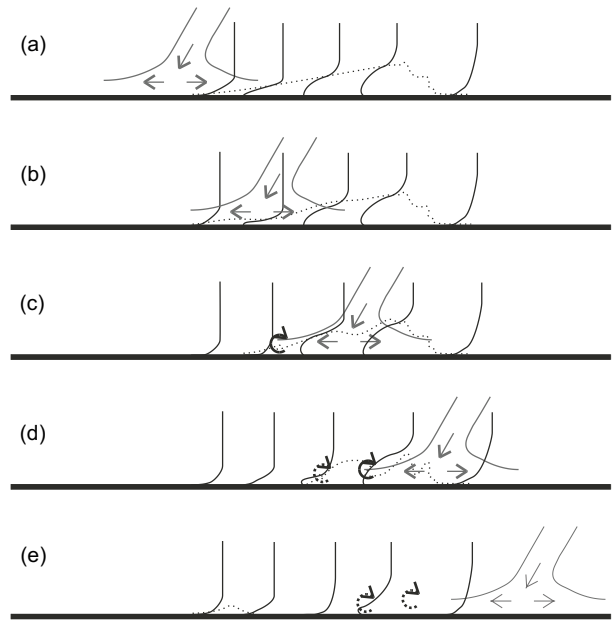


Figure 10: Sketch of rollup mechanism.

### SCHEMATIC OF WAKE INDUCED TRANSITION

Based on measurements presented thus far and the mechanism described above, a schematic of the wake induced transition process involving the interaction of a wake and separating boundary layer may be drawn as in Figure 11. The horizontal lines, labelled a - d, mark the phases shown in Figure 6 - Figure 9 respectively and the numbers used to identify features in these figures are transferred to Figure 11. The trajectory lines B and E are copied from previous ST diagrams.

Following the description of Halstead et al. [18], two generic transition paths may be identified on the blade surface. The wake-induced path and the transition path between wakes are indicated in Figure 11.

The wake-induced path differs from the traditional wake induced path for attached flow transition due to the interaction of the wake and separating boundary layer. The rollup of the separated shear layer into vortices that results from the interaction of the wake and inflexional profiles occurs by an inviscid mechanism. The diffusion of turbulence into the boundary layer is thus not a necessary precursor to the rollup of the shear layer and there is no time lag between the wake passing and the boundary layer response. The inviscid roll-up is represented in Figure 11 by a series of wedges originating beneath the centre of the wake at 4 and 5. The rollup vortices break down and a region of turbulent boundary layer follows the inviscid rollup process.

After the inviscid rollup of the shear layer, the wake turbulence diffuses into the boundary layer. This induces bypass transition in the attached boundary layer as described by Halstead et al. [18]. This bypass transition and the wake-induced transitional and turbulent strips occur along trajectory E of Figure 11.

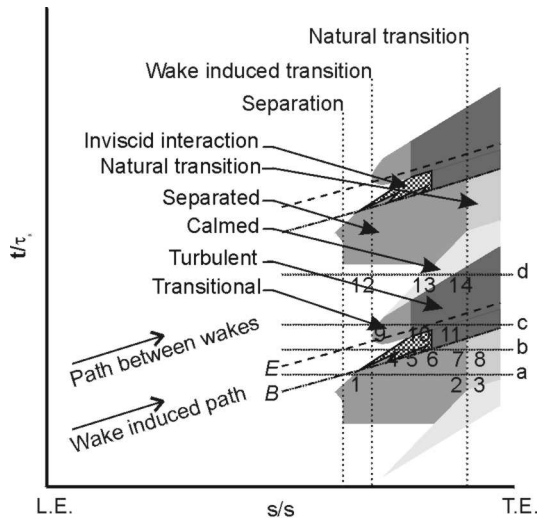


**Figure 11: Schematic of the transition mechanism resulting from the interaction of a wake and separating boundary layer.**

After the wake has passed, the stimulus for early transition is removed and the turbulent boundary layer upstream of the natural transition location relaxes to its pre-transition state. This is the transition path between wakes labelled in Figure 11. This relaxation process results in the calmed region, which is characterised by full velocity profiles that resist separation. The calmed region spreads as it convects downstream due to the different propagation velocities for the trailing edge of turbulent spots and the trailing edge of the calmed region. After the influence of the calming has decayed, the boundary layer profiles become inflexional and begin to separate under the adverse pressure gradient. The leading edge of this region of inflexional profiles initially follows the trajectory of the trailing edge of the calmed region. Thereafter, the inflexional or separating flow undergoes transition. The calmed region and early stages of separation are characterised by low levels of dissipation as shown by Stieger [19] and this is the loss reducing mechanism exploited by high-lift LP turbine blade designs. Immediately prior to the arrival of the wake, the separation location is observed to move fractionally upstream. This is the influence of the negative jet, which alters the pressure gradient locally and is a precursor to the inviscid rollup occurring beneath the wake.

## DISCUSSION

The transition mechanism described above is specific to conditions where wake induced bypass transition does not dominate the attached boundary layer flow upstream of separation point. For the formation of the rollup vortices to occur the separated laminar shear layer is required. This means that the Reynolds number and freestream turbulence must be low to permit separation. Furthermore, the wake passing frequency must not be so high as to prevent the boundary layer from beginning to separate between wake passing events.

The PIV measurements of Stieger et al. [17] identified rollup vortices embedded in the boundary layer. The preservation of these vortices in ensemble-averaged data is remarkable and emphasises the deterministic nature of the rollup mechanism resulting from the periodic wake passing. It is also notable that the flat plate boundary layer measurements of Stieger and Hodson [20] and the unsteady surface pressure measurements conducted by Stieger et al. [17] on this T106 cascade show that the natural transition occurring as the calmed region breaks down is also preserved through the ensemble average processing and is deterministic. The ensemble-averaging process does however remove the random unsteadiness and as a result the TKE levels are likely to be overestimated.

## CONCLUSIONS

The ensemble-average 2D LDA measurements of the boundary layer on the T106 LP turbine cascade provide new insight into the wake induced transition mechanism. The measurements show the separated shear layer associated with the inflexional profiles of the re-establishing separation bubble form rollup vortices beneath the passing wake. The vortices were formed by an inviscid Kelvin-Helmholtz mechanism. Due to the inviscid nature of the rollup mechanism, there was no delay between the wake passing and the boundary layer response. The rollup vortices were observed to breakdown into highly turbulent flow that convected along the blade surface.

The mechanism described above results when no wake induced turbulent spots are formed upstream of the separation location. The turbulent wake then convects over the inflexional profiles of the separating boundary layer and the inviscid breakdown described above results.

## ACKNOWLEDGMENTS

The first author would like to acknowledge the financial support of the ORS and a Peterhouse Research Studentship. The funding of EPSRC grant GR/L96660/01 is also gratefully acknowledged.

## REFERENCES

- [1] Schulte, V. and Hodson, H.P., 1994, "Wake-Separation Bubble Interaction in Low Pressure Turbines," AIAA/SAE/ASME/ASEE 30th Joint Propulsion Conference and Exhibit, Indianapolis, Indiana
- [2] Schulte, V. and Hodson, H.P., 1998, "Unsteady wake-induced boundary layer transition in high lift LP turbines," ASME Journal of Turbomachinery **120**, pp28-35
- [3] Curtis, E.M., Hodson, H.P., Baniaghbal, M.R., Denton, J.D. and Howell, R.J., 1996, "Development of blade profiles for low pressure turbine applications," ASME paper 96-GT-358
- [4] Howell, R.J., Ramesh, O.N., Hodson, H.P., Harvey, N.W., Schulte, V., 2000, "High Lift and Aft Loaded Profiles for Low Pressure Turbines," ASME 2000-GT-261

- [5] Cobley, K., Coleman, N., Siden, G., Arndt, N., 1997, "Design of new three stage low pressure turbine for BMW Rolls-Royce BR715 engine," ASME 97-GT-419
- [6] Haselbach, F., Schiffer, H-P., Horsman, M., Dressen, S., Harvey, N., Read, S., 2001, "The application of Ultra high Lift Blading in the BR715 LP Turbine," 2001-GT-0436
- [7] Brunner, S., Fottner, L., Schiffer, H-P., 2000, "Comparison of Two Highly Loaded Low Pressure Turbine Cascades under the Influence of Wake-Induced Transition," ASME 2000GT-268
- [8] Howell, R.J., Hodson, H.P., Schulte, V., Schiffer, H-P., Haselbach, F., Harvey, N.W., 2001, "Boundary Layer Development on the BR710 and BR715 LP Turbines - The Implementation of High Lift and Ultra High Lift Concepts," ASME Paper 2001-GT-0441
- [9] Wu, X., Jacobs, R.G., Hunt, J.C.R., Durbin, P.A., 1999, "Simulation of boundary layer transition induced by periodically passing wakes," J. Fluid Mech., **398**, pp109-153
- [10] Johnson, M.W., 2002, "Predicting Transition without Empiricism or DNS," GT-2002-30238
- [11] D'Ovidio, A., Harkins, J. A., Gostelow, J. P., 2001 a, "Turbulent spots in strong adverse pressure gradients: Part 1 - Spot Behavior," 2001-GT-0194
- [12] D'Ovidio, A., Harkins, J.A., Gostelow, J.P., 2001 b "Turbulent spots in strong adverse pressure gradients part 2- Spot propagation and spreading rates," 2001-GT-0406
- [13] Baniaghbal, M.R., Curtis, E.M., Denton, J.D., Hodson, H.P., Huntsman, I., Schulte, V., Harvey, N.W. and Steele, A.B., 1995, "Wake passing in LP Turbine Blades," presented at the AGARD conference, Derby, UK, 8.5-12.5
- [14] George, W.K., 1975, "Limitations to measuring accuracy inherent in the laser-Doppler signal," Proc. LDA Symp., Copenhagen
- [15] Meyer, R.X. 1958, "The Effects of Wakes on the Transient Pressure and Velocity Distributions in Turbomachines," ASME Journal of Basic Engineering, October, pp 1544-1552
- [16] Hodson, HP, 1998, "Bladerow Interactions In Low Pressure Turbines," in VKI Lecture Series No. 1998-02 Blade Row Interference Effects Axial Turbomachinery Stages, Von Karman Institute, Feb 9-12
- [17] Stieger, R.D., Hollis, D and Hodson, H.P., 2003 "Unsteady Surface Pressures due to Wake Induced transition in a laminar separation bubble on a LP turbine cascade," GT2003-38303
- [18] Halstead, D.E., Wisler, D.C., Okiishi, T.H., Walker, G.J., Hodson, H.P., Shin, H.-W., 1997 a, "Boundary layer development in axial compressors and turbines: Part I of 4 - Composite Picture," Journal of Turbomachinery, **119**, pp. 114-127
- [19] Stieger, R.D., 2002, "The Effects of Wakes on Separating Boundary Layers in Low Pressure Turbines," Ph.D. Thesis, University of Cambridge, Cambridge
- [20] Stieger, R.D., and Hodson, H.P., 2003, "Unsteady Dissipation Measurements on a Flat Plate Subject to Wake Passing," submitted to the 5<sup>th</sup> European Turbomachinery Conference, Prague